Decay study of ^{11}Be with an Optical TPC detector

N. Sokołowska,[1] V. Guadilla,[1] C. Mazzocchi,[1] R. Ahmed,[2] M. Borge,[3] G. Cardella,[4] A.A. Ciemny,[1] L.G. Cosentino,[5] E. De Filippo,[4] V. Fedosseev,[6] A. Fijałkowska,[1] L.M. Fraile,[7] E. Geraci,[8,4] A. Giska,[1] B. Gnoffo,[8,4] C. Granados,[6] Z. Janas,[1] Ł. Janiak,[1,9] K. Johnston,[10] G. Kamiński,[11] A. Korgul,[1] A. Kubiela,[1] C. Maiolino,[5] B. Marsh,[6] N.S. Martorana,[4] K. Miernik,[1] P. Molkanov,[12] J. D. Ovejas,[3] E.V. Pagano,[5] S. Pirrone,[4] M. Pomorski,[1] A.M. Quynh,[13] K. Riisager,[14] A. Russo,[5] P. Russotto,[5] A. Świercz,[15] S. Viñals,[3] S. Wilkins,[6] and M. Pfützner[1,*]

(ISOLDE Collaboration)

[1]*Faculty of Physics, University of Warsaw, 02-093 Warszawa, Poland*
[2]*National Centre for Physics, Islamabad, Pakistan*
[3]*Instituto de Estructura de la Materia, CSIC, Serrano 113-bis, E-28006 Madrid, Spain*
[4]*INFN-Sezione di Catania, Catania, Italy*
[5]*INFN-Laboratori Nazionali del Sud, Catania, Italy*
[6]*EN department, CERN, 1211 Geneva 23, Switzerland*
[7]*Grupo de Física Nuclear & IPARCOS, Universidad Complutense de Madrid, CEI Moncloa, E-28040 Madrid, Spain*
[8]*Dipartimento di Fisica e Astronomia "Ettore Majorana", Università di Catania, Catania, Italy*
[9]*National Centre for Nuclear Research, PL 05-400 Świerk-Otwock, Poland*
[10]*ISOLDE, CERN, 1211 Geneva 23, Switzerland*
[11]*Heavy Ion Laboratory, University of Warsaw, 02-093 Warszawa, Poland*
[12]*Institute covered by a cooperation agreement with CERN*
[13]*Nuclear Research Institute, 670000 Dalat, Vietnam*
[14]*Department of Physics and Astronomy, Aarhus University, DK-8000 Aarhus C, Denmark*
[15]*AGH University of Science and Technology, Faculty of Physics and Applied Computer Science, 30-059 Krakow, Poland*

(Dated: July 16, 2024)

The β decay of one-neutron halo nucleus ^{11}Be was investigated using the Warsaw Optical Time Projection Chamber (OTPC) detector to measure β-delayed charged particles. The results of two experiments are reported. In the first one, carried out in LNS Catania, the absolute branching ratio for β-delayed α emission was measured by counting incoming ^{11}Be ions stopped in the detector and the observed decays with the emission of α particle. The result of 3.27(46)% is in good agreement with the literature value. In the second experiment, performed at the HIE-ISOLDE facility at CERN, bunches containing several hundreds of ^{11}Be ions were implanted into the OTPC detector followed by the detection of decays with the emission of charged particles. The energy spectrum of β-delayed α particles was determined in the full energy range. It was analysed in the R-matrix framework and was found to be consistent with the literature. The best description of the spectrum was obtained assuming that the two $3/2^+$ and one $1/2^+$ states in ^{11}B are involved in the transition. The search for β-delayed emission of protons was undertaken. Only the upper limit for the branching ratio for this process of $(2.2\pm0.6_{\text{stat}}\pm0.6_{\text{sys}})\times10^{-6}$ could be determined. This value is in conflict with the result published in [Ayyad et al. Phys. Rev. Lett. 123, 082501 (2019)] but does agree with the limit reported in [Riisager et al., Eur. Phys. J. A (2020) 56:100]

I. INTRODUCTION

The isotope of beryllium $^{11}_{4}$Be has attracted the attention of both experimental and theoretical physicists for a long time due to a few interesting features. Contrary to the standard shell-model picture, its ground-state spin-parity is $1/2^+$ instead of $1/2^-$ [1, 2]. This spin inversion, which occurs due to residual interactions and provides an example of the disappearance of the $N = 8$ magic number, was spotted already in 1960 [3]. Effectively, it results from a migration of the $\nu 2s_{1/2}$ orbital below the $\nu 1p_{1/2}$ one. This, together with a low ground-state binding energy of 502 keV, is responsible for the single-neutron halo character of ^{11}Be [2, 4]. A further consequence is the unusually long half-life of ^{11}Be, $T_{1/2} = 13.76(7)$ s [5]. The full and detailed understanding of the parity inversion in this nucleus has been achieved only recently within *ab initio* theory by taking into account continuum effects and three-nucleon forces [6].

A part of the ^{11}Be decay scheme, which is of interest for the present work, is shown in Fig. 1. The delayed emission of α particles ($\beta\alpha$) was observed already in 1971 [7], but characterised with more details in Ref. [8], where the branching ratio for the $\beta\alpha$ channel was measured to be 2.9(4)% and the energy spectrum of α particles was explained by a single β transition to the $3/2^+$ state at 9.87 MeV in ^{11}B. A more precise and recent measurement of $\beta\alpha$ channel in the decay of ^{11}Be was published by Refsgaard et al. [9]. The value of the $\beta\alpha$ branching ratio was determined to be $b_{\beta\alpha} = 3.30(10)\%$. It confirmed that the $3/2^+$ state at 9.87 MeV dominates the $\beta\alpha$ spectrum, however, a better agreement with the data was obtained by inclusion of a second $3/2^+$ state at 11.49(10) MeV in ^{11}B.

In the decay of ^{11}Be also other delayed-particle channels are open, see Fig. 1. For the delayed emission of protons, tritons, and neutrons, the available energy windows are 281 keV, 286 keV, and 55 keV, respectively. The delayed emission of protons (βp) is of particular interest. It is a very well known process among neutron-deficient nuclei and a valuable source of nuclear-structure information for nuclei far from stability [11]. There are only a few neutron-rich nuclei, how-

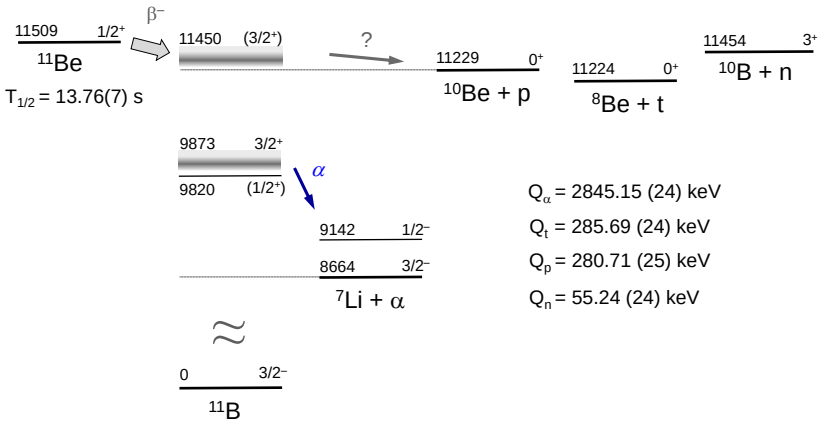

FIG. 1. Schematic decay scheme of ^{11}Be. Level energies (in keV) are given with respect to the ground state of ^{11}B. Only excited states in ^{11}B which are above the particle emission thresholds, and can be fed by allowed β decay, are shown, according to Ref. [5]. The Q-values for decays with emission of delayed particles were calculated using the AME 2020 mass evaluation tables [10].

ever, where this process can occur [12]. From the energy considerations it follows that the delayed emission of a proton after β^- decay is possible only when the available energy, $Q_{\beta p} = 782\,\mathrm{keV} - S_n$, is positive, where S_n in the neutron separation energy in the decaying nucleus [13]. Thus, low values of S_n are required, which makes the neutron halo nuclei the prime candidates [12]. In turn, the study of βp emission provides a tool to investigate the halo structure of the initial nucleus [14, 15]. The ^{11}Be is one of these candidates. The early theoretical prediction for its βp branching ratio in a two-body potential model yielded the value $b_{\beta p} = 3.0 \times 10^{-8}$ [12].

The experimental search for βp emission from ^{11}Be started 10 years ago at ISOLDE/CERN [15]. Due to the expected very small probability of this decay channel, a hybrid method was adopted. First, a sample of ^{11}Be was collected using ISOLDE mass separator. Then, the presence of ^{10}Be - the βp daughter of ^{11}Be - was searched for in the sample by means of accelerator mass spectrometry (AMS). The very first attempt did not yield a positive evidence with the branching $b_{\beta p} = (2.5 \pm 2.5) \times 10^{-6}$ [15]. The second approach, however, with the ^{11}Be source collection at ISOLDE and the AMS measurements made at the VERA facility at the University of Vienna, provided an unexpectedly high value of $(8.3 \pm 0.9) \times 10^{-6}$ [16].

The interest in the direct observation of β-delayed protons from the decay of ^{11}Be was suddenly boosted when the hypothesis of a dark decay channel of the neutron was put forward to explain discrepancies between the neutron lifetime measurements [17]. It was followed by an observation, that such a dark neutron decay could occur also in some nuclei with ^{11}Be being the most promising candidate [18]. Such a decay channel of this nucleus would lead to ^{10}Be, as claimed to be observed in Ref. [16], however, with no emission of protons. Soon afterwards, the direct emission of protons following the decay of ^{11}Be was reported by Ayyad et al. [19] who employed the Active Target Time Projection Chamber (AT-TPC) detector in an experiment performed at the ISAC-TRIUMF laboratory. The branching ratio was found to be $(1.3 \pm 0.3) \times 10^{-5}$, in agreement with the results of Ref. [16]. The observed energy distribution of protons indicated that the decay proceeds through a narrow resonance in ^{11}B at 11425(20) keV, with a total width $\Gamma = 12(5)$ keV and $J^\pi = (1/2^+, 3/2^+)$ [19]. These findings triggered a number of theoretical attempts to interpret such a cluster-like, narrow resonance close to the decay threshold [20–26]. The situation became less clear, though, when authors of Ref. [16] carried out another hybrid-like measurement in an attempt to reproduce their previous result. After special efforts to produce clean samples of ^{11}Be and a careful examination of potential contamination sources, Riisager et al. [27] concluded that the formation of ^{10}BeH$^+$ molecular ions in the ISOLDE ion source was a probable source of contamination in the previous experiment, leading to the surprisingly large $b_{\beta p}$ value. From the new measurement, only an upper limit for the βp branching ratio of 2.2×10^{-6} could be extracted [27]. On the other hand, new evidence for a narrow, near-threshold, proton-emitting resonance in ^{11}B, consistent with the results of Ref. [19] came from reaction studies [28, 29].

It appears evident, that further independent experimental studies are needed to verify the existence of the βp decay branch of ^{11}Be and, if confirmed, to clarify the puzzle of its strength. Guided by this motivation, and encouraged by a successful study of βd emission from ^{6}He [30], we undertook a study of ^{11}Be β decay using the Warsaw Optical TPC (OTPC) detector to record tracks of emitted charged particles. In contrast to the AT-TPC chamber used in Ref. [19], our detector was operated with a gas mixture of higher density which allowed us to observe the $\beta\alpha$ decay channel in the full energy range, from 200 keV to 3 MeV. Two experiments were performed. In the first one, at the INFN-LNS laboratory in Catania, the separated and identified in-flight ions of ^{11}Be were implanted into the OTPC one-at-a-time, and the following decays with emission of α particles were observed. This allowed us to determine independently the absolute branching

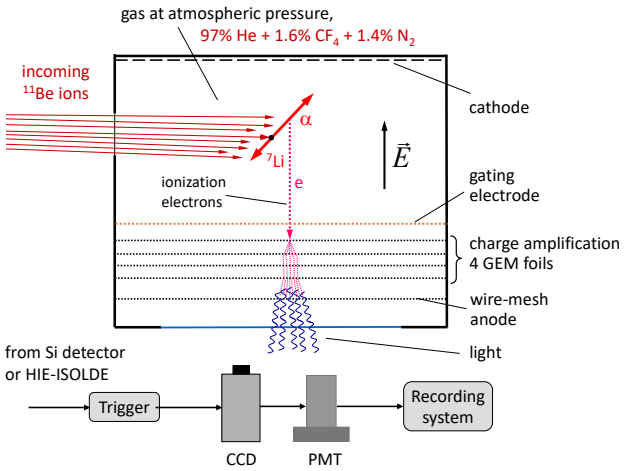

FIG. 2. Schematic representation of the OTPC detector and its working principle.

ratio for the $\beta\alpha$ channel. The second experiment was made at HIE-ISOLDE at CERN. Reaccelerated bunches containing a large, but unknown number of ^{11}Be ions were implanted into the OTPC followed by observation of their decays. A large number of $\beta\alpha$ events allowed to establish the energy spectrum for this channel with a different method than the one used by Refsgaard et al. [9]. This provided a check of the energy calibration of our chamber and, together with the $\beta\alpha$ branching ratio, the absolute normalisation for the number of implanted ^{11}Be ions. The large statistics accumulated in this measurement was sufficient to look for the βp decay channel at the level of 10^{-6}. In this paper, we present the results of both experiments.

II. EXPERIMENTAL TECHNIQUES

A. The OTPC detector

The OTPC detector was developed at the University of Warsaw to study rare decay modes with emission of charged particles, like $2p$ radioactivity and β-delayed multi-particle emission. More details on this instrument are given in Ref. [31] and the newest, upgraded version is described in Ref. [32]. Here we summarize briefly the principle of operation with a focus on features relevant to this work. The scheme of the detector is shown in Fig. 2.

In the reported experiments, the detector was filled with a gaseous mixture of 97% He, 1.6% CF_4, and 1.4% N_2 at atmospheric pressure. Within the active volume, between the cathode and the amplification stage, a constant and uniform electric field of 143 V/cm in the vertical direction was maintained. Ions enter the active volume horizontally, through a kapton window. Primary ionization electrons, generated by the stopping ion and by charged particles emitted in its decay, drift with a constant velocity v_d towards the amplification stage, passing first through a wire-mesh gating electrode. By changing the potential of this electrode the sensitivity of the detector can be modified. This feature is used to reduce or block the large charge generated by heavy ions. The charge amplification is realized by four gas electron multiplier (GEM) foils [33]. Below the GEM section, there is the final wire-mesh anode. In the space between the last GEM foil and the anode, the electric signal is converted to light. The light is recorded with a CCD camera and a photomultiplier (PMT) connected to a digital oscilloscope with the 50 MHz sampling frequency. The CCD image represents a projection of an event on the anode plane, integrated over exposure time, while the PMT waveform provides the total light intensity as a function of time. The latter contains the information on the event along the direction of the electric field, i.e. perpendicular to the anode plane. The combination of data from the CCD and the PMT allows the reconstruction of the decay event in three dimensions, provided no particle escaped the active volume. In front of the OTPC entrance window, an aluminium degrader of variable thickness is mounted to optimize the implantation depth of the ions of interest. In addition, during the experiment at the LNS, a Si detector of 140 μm thickness was placed in front of this degrader. It provided an additional energy-loss signal, ΔE, used to confirm the particle identification.

The gas flowing out of the OTPC was passing through another small gas chamber where the electron drift velocity was measured. The same value of the electric field was maintained to ensure the same conditions as in the OTPC. The average value of the v_d was found to be 9.20 mm/μs and 9.36 mm/μs for the LNS and ISOLDE experiments, respectively.

B. Experiment at LNS

The measurement was performed in the Laboratori Nazionali del Sud of INFN (INFN-LNS) in Catania, Italy, at the in-Flight Radioactive Ion Beams (FRIBs) facility [34, 35]. Ions of ^{11}Be were produced by the fragmentation reaction of a ^{13}C primary beam, delivered by the Superconducting Cyclotron (SC), impinging on a 1.5 mm thick beryllium target at the energy of 55 MeV/nucleon. The reaction products were purified in a separator composed of two 45° dipole magnets and a homogenous aluminium 1 mm thick degrader mounted between them. The main feature of this production method, of key importance for this work, is the possibility of full identification in-flight of single ions coming out of the separator. This was accomplished by the ΔE–TOF technique. The energy-loss (ΔE) information was provided by a 70 μm thick DSSSD detector, mounted at the entrance to the so-called 0° experimental hall, where the OTPC detector was installed. The time-of-flight (TOF) measurement was started by the Radio Frequency (RF) signal from the SC and stopped by signals from the DSSSD strips. The resulting identification plot is shown in Fig. 3. The main group of events represents ions of ^{11}Be, while small contamination comes from ions of ^{9}Li. The average rate of ^{11}Be was about 200 ions/s.

The main goal of the experiment at the LNS was to remeasure the branching ratio $b_{\beta\alpha}$ for the $\beta\alpha$ emission from ^{11}Be. Since identified in-flight single ions were being implanted into

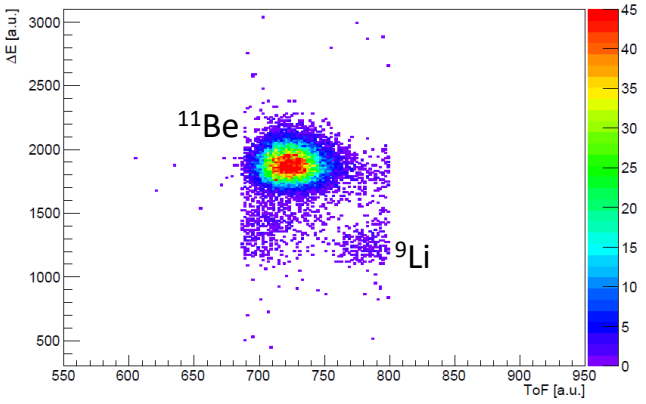

FIG. 3. (Color online) The ΔE–TOF identification plot of ions delivered by the separator from the FRIBs acquisition system. Contaminant ions of ^{9}Li are seen on both sides of the measured TOF band due to periodic condition implied by using the RF signal for the time reference.

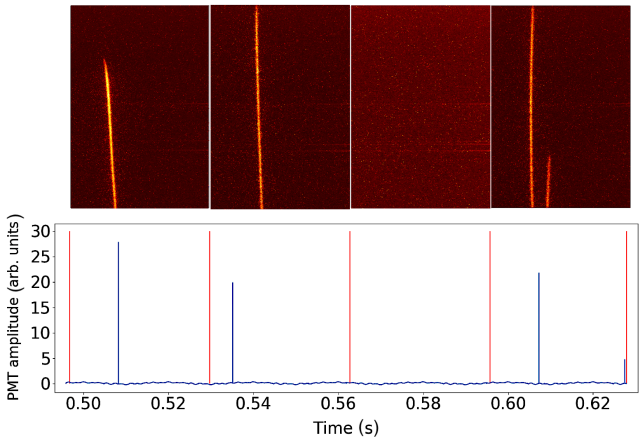

FIG. 4. (Color online) Example of data taken at the LNS. The first few CCD images (top) with the corresponding PMT waveform (bottom) showing the ions entering the OTPC detector. Time values separating individual CCD frames are marked on the PMT waveform with red lines. In the first and the fourth frame, a stopped ion can be seen.

the OTPC, the $b_{\beta\alpha}$ could be determined by counting the number of stopped ions and the number of decays with the emission of α particle. Due to a large momentum spread of ^{11}Be ions, being a consequence of the fragmentation reaction in a relatively thick target, the range distribution of these ions was broader than the gas thickness of the OTPC. To determine the fraction of ^{11}Be ions stopped in the active gas section of the detector, a dedicated measurement was made, where ions, implanted into the OTPC in an uninterrupted way, were counted. The CCD was operated in a cycle of taking 27 images, each with the 33 ms exposure, followed by a 5 s break to save the data on the disk. The PMT was recording the light continuously over the time of all 27 images. An example showing the beginning of such a "movie" is given in Fig. 4. In this part of the experiment more than 100 thousand CCD images were collected.

A different detection cycle was used in the runs where $\beta\alpha$ decay events of ^{11}Be were counted. Using a special low-energy chopper, at the ion source of the SC, the beam was delivered to the OTPC only in short periods of 750 ms, every 60 s. After such implantation period, the OTPC acquisition system was started. A series of 63 CCD images, of 33 ms exposure each, was recorded, while the PMT was recording light continuously over the time of all these images. This set was followed by a 1.2 s break to save the data on the disk. Such a sequence was repeated 8 times. Thus, the collection of the decay data lasted about 26 seconds. In the remaining 34 seconds of the beam cycle no data were recorded. This time was set to make sure that most of the stopped ions will decay before the next bunch of ions is implanted. As an example, a part of the decay data is shown in Fig. 5. In total, almost 4 million CDD images were collected in this part of the experiment.

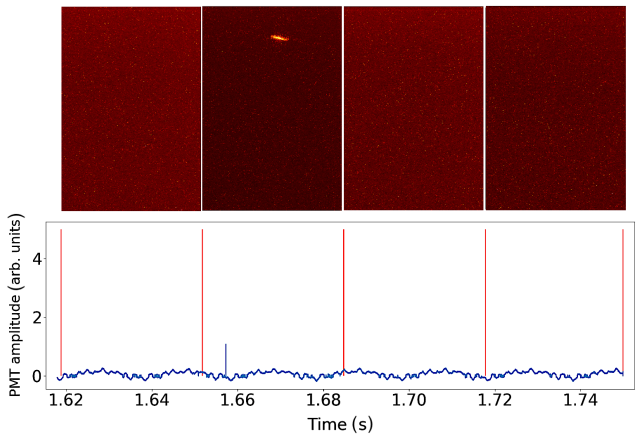

FIG. 5. (Color online) Example of date taken at the LNS. The first few CCD images (top) with the corresponding PMT waveform (bottom) showing the decays of ^{11}Be ions stopped during the preceding beam-on period in the OTPC detector. Time values separating individual CCD frames are marked on the PMT waveform with red lines. Only in the second frame, a decay event is observed

C. Experiment at HIE-ISOLDE

The ^{11}Be beam was produced at the ISOLDE facility at CERN [36, 37] and post-accelerated at the HIE-ISOLDE accelerator [38]. The 1.4 GeV protons from the PS Booster accelerator were directed onto a UCx target equipped with a tantalum hot cavity. Beryllium isotopes were laser ionised using the RILIS ion source [39] and accelerated to 30 keV before being mass separated by the general-purpose mass separator. For the beam to be post-accelerated, it was injected first into a Penning trap (REXTRAP), where the beam was bunched, and then into an electron beam ion source (EBIS) where the singly charged ^{11}Be was charge-bred to ^{11}Be^{4+} with a breeding time

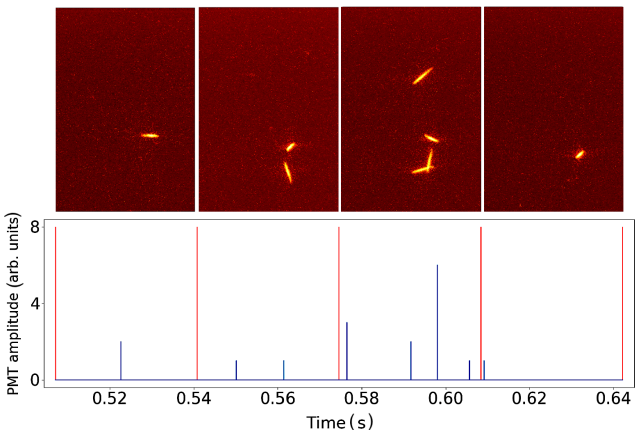

FIG. 6. (Color online) Example of data taken at the HIE-ISOLDE. The first few CCD images (top) with the corresponding PMT waveform (bottom) showing decays of ^{11}Be ions stopped during the preceding beam-on period in the OTPC detector. Time values separating individual CCD frames are marked on the PMT waveform with red lines.

of 46 ms. The beam, with $A/q = 2.75$, was subsequently injected into a linear post accelerator where an eventual energy of 7.5 MeV/nucleon was achieved. To remove ions of ^{22}Ne^{8+}, which were present as an impurity from the EBIS, carbon stripping foils were employed allowing a very clean beam of ^{11}Be to be delivered, via the XT03 beam line, to the experimental station where the OTPC detector was installed.

The detection cycle was similar to the one used at LNS for the decay data collection. It started with the opening of the beam gate for 750 ms during which ^{11}Be ions were implanted. Afterwards, the OTPC acquisition system was started. A series of 63 CCD images, with 33 ms exposure, were taken while the PMT was recording the light continuously during this time. A break of 1.2 s followed, to save the data on disk. This sequence was repeated 4 times, yielding a total detection time of about 12 s. For the next 48 s, no data were recorded. After the 60 s from the start the next bunch of ions was accepted and the new detection cycle was started. An example of the collected data is shown in Fig. 6.

III. DATA ANALYSIS

A. Single-ion implantation

Data collected in the LNS experiment allow us to determine the number of ^{11}Be ions stopped inside the detector and count the number of decays with emission of charged particles. From these, the branching ratio for β-delayed α emission can be calculated.

The first part of the LNS run was used to establish the percentage of ions stopped in the OTPC. An automatic counting procedure was developed for this purpose. Each CCD image was divided into 10 horizontal slices along x-axis (perpendicular to the beam direction). The content of each slice was projected on the x-axis. An algorithm based on a peak searching routine was applied to each slice in order to perform tracking of the ion trajectories, allowing the determination of the end of the track for those ions stopped inside the chamber. The good performance of the routine was verified in a subset of data. The PMT waveform corresponding to the CCD image was used to cross-check the number of ion tracks found by the algorithm. From the results obtained, the number of ions entering the OTPC and the number of ions stopped within the active volume was determined. After applying this procedure to all CCD frames in this part, the final average probability of stopping an ion in the OTPC was found to be 19.4(27)%. Events with a mismatch between the number of tracks in the CCD and the PMT data represent the main contribution to the error. The distribution of the y coordinate of the stopped ions (range distribution in the OTPC gas) was found to be almost flat, in agreement with the calculations made with the LISE^{++} ion-optical simulation tool [40].

The final identification of ions entering the OTPC detector was made with the help of the Si detector mounted in front of the chamber. The ID plot obtained with this detector was essentially the same as the one provided by the DSSSD detector used by the standard FRIBs acquisition system, shown in Fig. 3. Since some ions could have been stopped in materials between the Si detector and the active gas volume (variable Al degrader, entrance window), the counting of ions entering the OTPC was made by applying a coincidence condition between the signal from the Si detector and the light detected in the OTPC by the PMT. From the resulting ID plot, it was found that ^{11}Be ions represented 93(1)% of ions entering the OTPC. The remaining 7% corresponded to ions of ^{9}Li.

In the second part of the LNS experiment, the information on ^{11}Be decays was recorded. From the ID data collected during this part, we counted 633 501 ions, which entered the OTPC detector. After the correction for beam purity and stopping probability, about 114300 ions of ^{11}Be were found as stopped inside the detector. Most of the 4 million CCD images taken in this part were empty. A selection of frames (about 10^5) containing a clear signal above the noise was chosen for further analysis. A majority of them showed a track of α particle from a weak diagnostic α source installed inside the OTPC, composed of ^{243}Cm, ^{243}Am, and ^{241}Am. These tracks were easy to discern because they emerged from the well-defined region on the left border of the image and their length was much longer than the longest tracks expected in the decay of ^{11}Be. Another type of events originated from natural radioactive decay chains, which included α emitters. They could be also distinguished from the ^{11}Be decays by the much larger energy, and thus the track length. The third source of background was represented by the point-like, short light flashes on the GEM foils. They were easy to identify due to the small size of a few pixels on the CCD image and a very short signal of a few samples in the PMT waveform. A dedicated selection tool was developed which scanned all recorded frames and using the characteristics mentioned above removed the frames containing these background events. After this procedure, 1837 decay events remained. Among this number some events may come from decays of

the contaminant ^{9}Li which has a 50% branch of β-delayed neutrons, leading to two α particles in the final state [41]. Since the half-life of ^{9}Li is only 178 ms, decays of any stopped ^{9}Li will happen within the first sequence of 63 CCD images (the first "movie") in the decay-detection cycle which lasts 2.079 s (see Section II B). To avoid this contamination, we dismissed 380 decay events which were found to occur in the first "movie". Because the branching ratio for the delayed emission of protons in ^{11}Be is more than 3 orders of magnitude smaller than that for the emission of α particles, we can safely assume that the resulting number of 1457 decay events represents only $\beta\alpha$ emission from ^{11}Be. As the observation time of decays was finite, the corresponding correction must be introduced. Taking into account the detailed timing cycle of the decay measurement, with the first "movie" removed, and the half-life of ^{11}Be, the probability of recording an $\beta\alpha$ decay was 39.0(1)%.

Taking together relevant numbers and correction factors, we arrive at the branching ratio for β-delayed α emission, $b_{\beta\alpha}$ = 3.27(46)%. It agrees very well with the value of 3.30(10)%, reported in Ref. [9], albeit is less precise. The uncertainty of our value is dominated by the uncertainty of the probability of stopping ions in the OTPC detector.

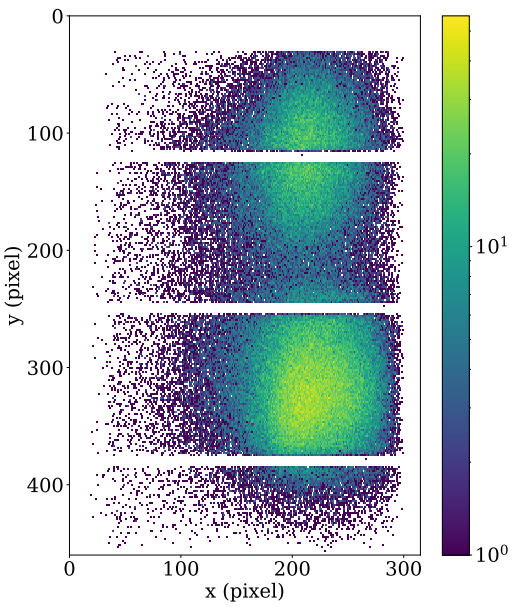

FIG. 7. (Color online) Position distribution of selected ^{11}Be decay events on the CDD plane in the HIE-ISOLDE experiment. One pixel corresponds to 0.63 mm. See text for more explanations.

B. Decay events

The number of decay events collected during the LNS experiment was too small for the analysis of the $\beta\alpha$ energy spectrum. This goal can be achieved by the analysis of data from the HIE-ISOLDE experiment where much larger statistics of ^{11}Be decays was gathered. In total about one million CCD images were taken but, in contrast to the LNS experiment, many frames contained two or more decay events. In these cases, there is no general unambiguous way to decide which event seen on the CCD image corresponds to which decay signal in the PMT waveform. That is why we selected only frames exhibiting one decay event for the further analysis. There were about 270 thousand such frames.

In the next step, each CCD frame was analysed by a procedure detecting the position of the event on the image, and in particular determining the positions of both ends. All events, where the position of one of the ends of the track resulted to be closer than 2 cm from the wall, were discarded. This is because close to the walls the electric field is less homogeneous and thus the reconstruction of such events is less reliable. In addition, we have to take into account that the GEM foils used in the OTPC are composed of four sections which are separated electrically by a narrow inactive strip which stops drifting electrons. As a consequence, on the image plane there are three horizontal narrow bands with strongly reduced sensitivity. The events which were found to overlap with one of these bands were also discarded. The resulting position distribution of the decay-event centers, on the image plane (x, y), is shown in Fig. 7. The decays can be seen to concentrate in two separate regions which correspond to two locations in the detector where the incoming ions were stopped. This is caused by the OTPC entrance window which is covered with horizontal strips of 5 μm of copper and 2 μm of gold used to maintain the uniform electric field in the chamber. The strips are 7 mm wide with 3 mm space in between. Although the energy of the ^{11}Be beam was well defined, the beam spot on the OTPC window was broader than one strip, so that ions passing through the additional strip material lose more energy, and thus have a shorter range in the gas than ions passing between the strips. We cannot determine the decay position in the vertical (z) direction, so some decays can happen close to the cathode or the GEM section and may appear deformed or damaged. Due to diffusion, the probability of finding an ion far from the implantation point, in all directions, increases with time and about 5% of ions implanted in one detection cycle can survive more than 1 minute and decay within the next cycle. To partly moderate this effect, we decided to discard events having the position coordinate $x < 100$ pixels, see Fig. 7.

Since the β-delayed emission in ^{11}Be happens almost at rest, the particles are emitted in opposite directions (back-to-back) forming a single, straight track, as can be seen in Figs. 5 and 6. The reconstruction of each event in three dimensions is done by extracting the ionisation distribution along this track and by comparing it with the energy loss model. First, the relevant parts containing the decay signal were isolated from the PMT waveform and from the CCD image of each event. A rectangular part containing the track was cut out from the image and its content was projected, in the image plane, on the direction along the track, and on the direction perpendicular to it. The former projection was very well approximated by a Gaussian curve with the width parameter σ_{CCD} describing all effects of electron diffusion, in the drift and the amplification sections, in the horizontal plane of the detector. The latter pro-

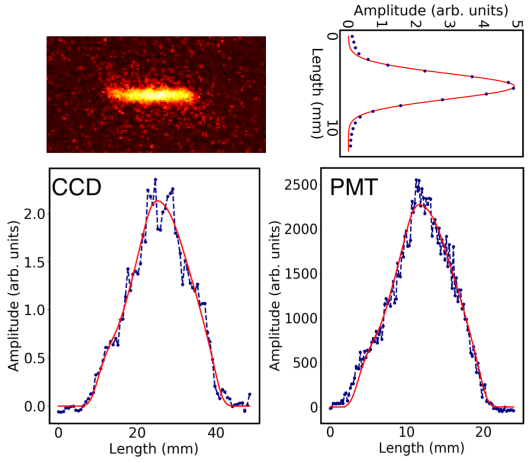

FIG. 8. (Color online) Example data for one decay event of ^{11}Be. Top left: a part of the CCD image showing the event track; top right: the projection of the image part on the axis perpendicular to the track with the best-fitted Gaussian curve (red line); bottom left: the projection of the image part on the axis parallel to the track; bottom right: the corresponding part of the PMT signal representing the vertical component in the length scale. The red lines in the bottom panels show the best-fitted model signal corresponding to a $\beta\alpha$ event with the decay energy of 1140 keV and the emission angle of the α particle of 28° with respect to the horizontal plane.

jection represented the ionisation distribution along the track as seen on the horizontal plane. An example result for one decay event is shown in Fig. 8.

In the analysis, we consider two decay scenarios: delayed emission of α particle ($^{11}\mathrm{B}^* \rightarrow {}^{7}\mathrm{Li}+\alpha$) and delayed emission of a proton ($^{11}\mathrm{B}^* \rightarrow {}^{10}\mathrm{Be}+p$). The predictions for the ionization profile along the track were done using two models for the energy loss of charged particles in matter.

The first one is the model included in the SRIM package [42], commonly adopted in similar applications. The second one is the low-energy model included in the GEANT4 simulation toolkit [43], employing the ICRU49 parameterisation of evaluated data for stopping powers [44]. The use of the latter was necessary, as we used GEANT4 to make realistic simulations of our data events to verify the reconstruction procedure, as described below. With these models we first computed the ranges of particles in the OTPC gas, as a function of their energy, see Fig. 9. Having these functions, one can calculate the energy deposited along the track for the given decay energy. By the energy deposit we mean here the energy lost by ionization of gas atoms - this caveat is important especially at the end of the track, where the stopping power is dominated by nuclear collisions which do not liberate electrons. Assuming the emission angle with respect to the image plane (x, y), one can determine the expected distributions of the energy deposit in the two measured projections of the track. In the final step, before the comparison with the data, these predicted distributions are folded with the Gaussian curves accounting for the diffusion of the primary ionisation electrons during the drift time and the spread due to electron multiplication in the GEM section. For the horizontal projection, the σ_{CCD} value, extracted from the image, was taken. For the vertical projection the corresponding σ_{PMT} value was considered as a free parameter in the minimization process. Examples of total energy-loss model distributions with segregated contributions from both particles are shown in Fig. 10. For each decay event, and for both decay scenarios, a least-squares minimization procedure was applied to find the decay energy, emission angle with respect to the horizontal (x, y) plane, and σ_{PMT} best describing the measured distributions. It was done by minimizing the chi-square function:

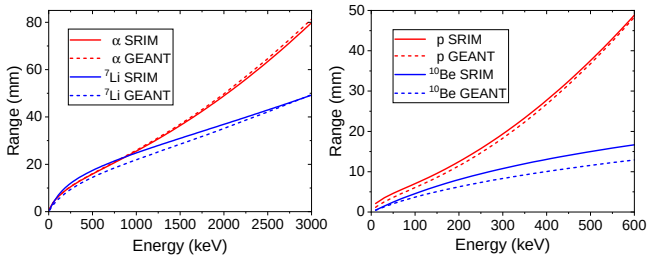

FIG. 9. (Color online) Ranges of particles in the OTPC gas mixture used in the HIE-ISOLDE experiment, as a function of particle energy, as predicted by the SRIM [42] and the GEANT4 [43] models.

$$\chi^2 = \sum_{i=1}^{n}\left(\frac{d^i_{\mathrm{CCD}} - m^i_{\mathrm{CCD}}}{\delta_{\mathrm{CCD}}}\right)^2 + \sum_{i=1}^{m}\left(\frac{d^i_{\mathrm{PMT}} - m^i_{\mathrm{PMT}}}{\delta_{\mathrm{PMT}}}\right)^2, \qquad (1)$$

where the first (second) sum runs over the n (m) data points of the CCD (PMT) signal. With d^i_c and m^i_c the values of the i-th data point and the model are denoted, respectively, while δ_c represents the uncertainty of the data in the channel c (CCD or PMT). For the uncertainties, the following approximation was adopted:

$$\delta_c^2 = \frac{\sum_{i=1}^{n}\left(d^i_c - d^i_{\mathrm{smooth}}\right)^2}{n}, \qquad (2)$$

where the d_{smooth} is the result of smoothing the d_c data set with a Gaussian filter. An example result of this minimization procedure is shown in Fig. 8.

To verify the reconstruction procedure described above, and to gauge its performance, we used the GEANT4 package [43] to make simulations of the observed decay events. The real conditions in the OTPC were assumed and the distribution of the energy deposited was simulated for a given decay type, decay energy, and emission angle in the 3D space. Then, the resulting distribution was diffused both in horizontal and vertical directions using realistic widths. Finally, it was projected on the (x, y) plane, and on the z direction, taking into account the pixel size of the CCD image (0.63 mm), and the binning of the PMT signal (equal to $v_d \times 20$ ns), respectively. A noise distribution, sampled from the experimental data, was added to both output files. This procedure yields a CCD-like image file and a PMT-like waveform, providing a realistic representation of a decay event, for which the physical parameters are known. More details of the simulation procedure are given

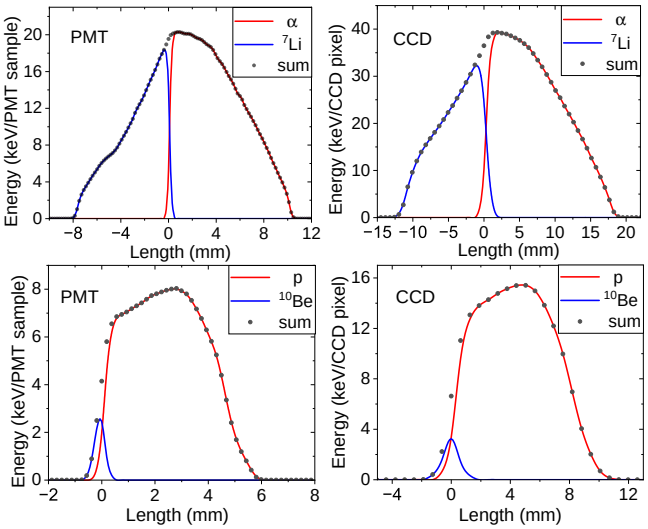

FIG. 10. (Color online) Predicted energy deposition profiles calculated with the SRIM model for the decays of ^{11}Be in the OTPC gas in the HIE-ISOLDE experiment. Top: decay into α+^{7}Li for the decay energy of 1200 keV and the α emission angle of 30° with respect to the horizontal plane. Bottom: decay into p+^{10}Be for the decay energy 200 keV and the proton emission angle of 30°. On the left the vertical projections are shown, as seen in the PMT signal, on the right the profiles along the track projected on the horizontal plane are shown, as extracted from the CCD image. All curves were diffused with $\sigma_{PMT} = \sigma_{CCD} = 2$ samples/pixels.

in Ref. [45]. The simulated events are reconstructed in exactly the same way as the real data, using the above-mentioned GEANT4 model of energy loss and the determined parameters can be compared to the input ones.

A set of simulations of the ^{11}Be $\beta\alpha$ decay was made for energies in the full energy range, assuming isotropic emission. In general, the reconstruction procedure was found to reproduce the key input parameters very well. In particular, the response of the reconstruction to the simulated monoenergetic decays was studied systematically. A set of $\beta\alpha$ events was simulated for well-defined energies in the range from 100 keV to 2.8 MeV and for isotropic emission in space. After reconstruction, each monoenergetic group was found in a Gaussian-like distribution with its maximum equal to the input energy and the width (σ) of about 25 keV, slightly decreasing with increasing energy, as can be seen in Fig. 11. The emission angles were found to be reproduced with an accuracy of about 1 degree. Results obtained in this part were used to construct a response matrix representing the distortions of the real spectrum induced by the data analysis.

In the process of data reduction, as described above, decay events close to the walls, as well as events found to run across one of the three gaps in the active GEM area (see Fig. 7), were discarded. The probability of being affected by this process, however, depends on the length of the track, and thus on the decay energy. To figure out this dependence, other Monte Carlo simulations were done. The distribution of decaying ^{11}Be ions was assumed to be composed of two clouds approximated by three-dimensional Gaussian distributions. The

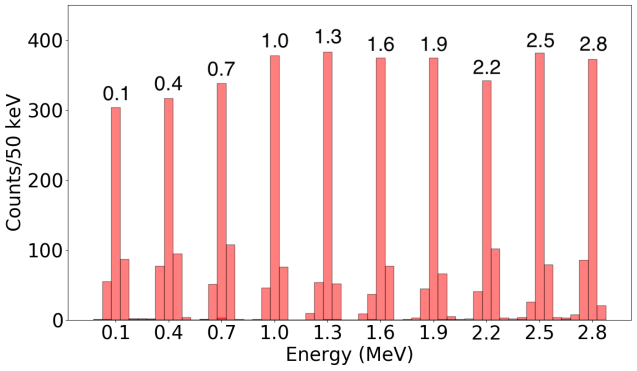

FIG. 11. Results of reconstruction for a set of simulated monoenergetic $\beta\alpha$ decay events. Each peak corresponds to events of the same input energy shown by the label.

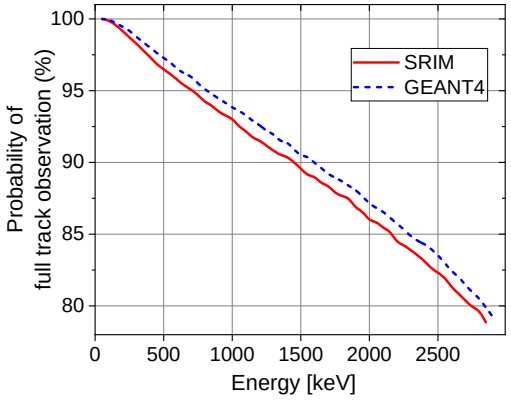

FIG. 12. (Color online) Observation probability of the full track of a $\beta\alpha$ decay event in the OTPC detector in the HIE-ISOLDE experiment as a function of decay energy.

width parameters of these distributions in the x and y directions were read out from the data (Fig. 7). The width in the z direction was assumed to be the same as in the x direction. For a given decay energy, the decay location was sampled randomly from this distribution, together with the emission angle assuming isotropic decay. Then, taking into account the detector dimensions, it was checked whether the event would be rejected because of proximity to a wall or because of coming into a dead gap in the GEM foil. This procedure was executed separately for the SRIM and the GEANT4 energy loss models. The probability to observe the full event, determined in such a way, as a function of decay energy, is shown in Fig. 12.

IV. RESULTS

A. Spectrum of β-delayed α particles

Each event was reconstructed using both $\beta\alpha$ and βp scenario yielding the minimized chi-square values, χ^2_α and χ^2_p, respectively. In Fig. 13 the chi-square difference, $\Delta\chi^2 = \chi^2_\alpha - \chi^2_p$,

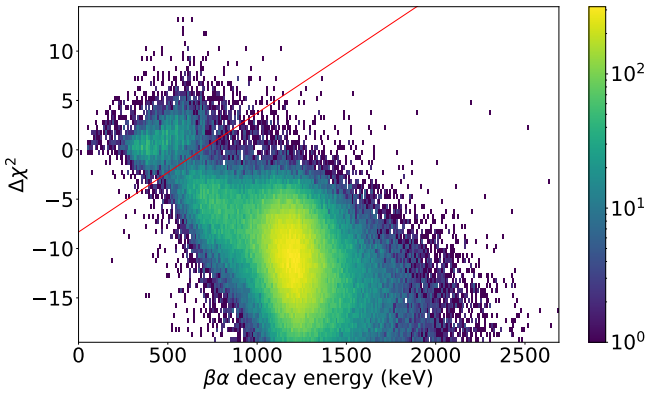

FIG. 13. (Color online) The difference between the minimised chi-square values obtained in the reconstruction procedure of each event assuming the $\beta\alpha$ and the βp decay ($\Delta\chi^2 = \chi^2_\alpha - \chi^2_p$), as a function of decay energy for the $\beta\alpha$ scenario. The SRIM energy-loss model was used. Only events located below the red line were included in the $\beta\alpha$ spectrum.

as a function of decay energy for the $\beta\alpha$ decay and for the SRIM model is shown. Events having $\Delta\chi^2 < 0$ were fitted better as representing $\beta\alpha$ process, while those with $\Delta\chi^2 > 0$ are better reconstructed as βp events. In Fig. 13 we can see a well separated group of events at low energy with values $\Delta\chi^2 \gtrsim 0$. It contains about 7 thousand events, which corresponds to about 3% of all statistics. Thus, they cannot represent entirely the delayed proton emission because of their number and also because of the energy, exceeding the Q_p value. All these events were inspected one-by-one and it was found that most of them were showing a clear sign of damage, most often a cut. We believe that they represent $\beta\alpha$ decays which occurred close to the cathode or to the GEM section. Some of them could originate from ^{11}Be ions that were not fully neutralized and drifted to the cathode before decaying. Many of these events were cut from both sides, suggesting a decay between the GEM foils. The reason for such events being fitted better as βp decays is that when the energy deposition profile of the $\beta\alpha$ event is cut, it may become similar to the proton emission profile (see Fig. 10). The red line in Fig. 13 marks the bottom of the "valley" between two groups of events given by the local minimum of counts. We decided to discard all events located above the red line in Fig. 13 from the analysis of the $\beta\alpha$ spectrum.

The distributions of reconstructed decay energy and emission angle for accepted 225 482 $\beta\alpha$ events, using the SRIM model, are shown in Fig. 14. As long as decays occur within the detector volume, emission of delayed particles should be isotropic. Indeed, the measured angular distribution is very close to isotropic for the absolute value of the emission angle above 30°, see Fig. 14b. A problem appears, however, at small angles: there are too many events at small negative angles, while there are clearly missing events with small positive angles. When particles are emitted at a small angle i.e. almost parallel to the x, y plane, the information on the angle is encoded in the details of the PMT signal. For the zero angle this signal should be symmetric and Gaussian-like. Then, however, the PMT sees a strong, short pulse of light and non-linearities in the charge processing slightly distort the shape of the output signal. This is interpreted by the reconstruction procedure as resulting from a small, non-zero angle. For larger angles, the shape details are much less important, as the lengths of the horizontal and vertical components carry the main information about the angle. The erroneous determination of small angles should have a small influence on the event energy, as in such case it is encoded mainly in the length of the track which to the first order does not depend on the angle. Nevertheless, in the analysis of the energy spectrum, we do check how the final results are affected by the removal of events with incorrect angles. Note that with GEANT4 isotropically simulated events, where no PMT signal distortions are taken into account, the angular distribution reconstructed with the same procedure as experimental data did not present any distortion at small angles.

In addition, the whole reconstruction procedure of accepted $\beta\alpha$ events was repeated using the GEANT4 energy-loss model. The distribution of χ^2_α was found broader than in the case of the SRIM model, indicating worse reconstruction quality in general. The resulting energy spectrum was found to have a very similar shape to the one stemming from the SRIM model, although shifted by about 15 keV towards lower energies. The angular distribution was found also asymmetric, very much like the one shown in Fig. 14b, however, reversed with respect to zero angle. Due to small differences in the range curves (Fig. 9), the predicted energy deposition profiles by the GEANT4 model are slightly different than those from SRIM. As a result, the asymmetries present in the PMT signal for events with an angle close to zero are interpreted by the GEANT4 model in the opposite way. In the following, we will analyse only the $\beta\alpha$ spectrum obtained with the SRIM model.

B. *R*-matrix analysis

The $\beta\alpha$ spectrum was analysed within the *R*-matrix framework [46], following the approach taken by Refsgaard et al. [9]. We consider only Gamow-Teller transitions to $1/2^+$ and $3/2^+$ levels in ^{11}B, denoted in the following by the index λ. Each level is characterised by its energy E_λ, β-decay feeding factor B_λ, and its reduced width amplitudes $\gamma_{\lambda c}$, which are considered as free parameters in the fitting procedure. The decay channel, c, denotes the final state in ^{7}Li ($c = 1$ for the ground state and $c = 2$ for the $1/2^-$ excited state at 478 keV). The decay energy spectrum is given by [47]:

$$N(E) = \sum_c N_c(E),$$
$$N_c(E) = f_\beta P_c \left| \sum_{\lambda\mu} B_\lambda \gamma_{\lambda c} A_{\lambda\mu} \right|^2, \quad (3)$$

where f_β is the phase space factor for the β decay, P_c is the barrier penetrability [46], and $A_{\lambda\mu}$ is the level matrix defined in Ref. [48]. The phase-space function f_β was calculated with the LOGFT tool provided by the NNDC portal [49]. For the

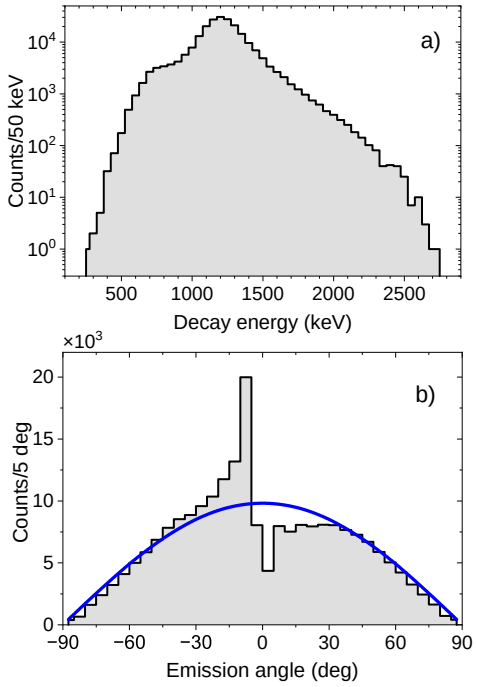

FIG. 14. Reconstruction results of $\beta\alpha$ events for the SRIM energy-loss model. a) Energy spectrum, b) corresponding distribution of the emission angle. The smooth line shows the cosine function, expected for isotropic emission.

Coulomb wave functions, necessary to calculate the P_c and $A_{\lambda\mu}$ terms, we used the formulation given in Ref. [50]. For the channel radius parameter, we adopted $r_0 = 1.6$ fm and we took into account only p-wave α emission ($l = 1$) following Ref [9].

For given values of fitting parameters, the model spectrum was calculated with Eq. 3 and corrected by the analysis response matrix and for the probability of observing the full track (Fig. 12). Then, the Poisson likelihood chi-square value was computed [51]:

$$\chi^2_L = 2\sum_i \left[y_i - n_i + n_i \log\left(\frac{n_i}{y_i}\right)\right], \qquad (4)$$

where n_i and y_i are the number of counts in the i-th data bin and the number of counts predicted by the model for this bin, respectively, and the sum runs over all data bins. The minimization of χ^2_L was done using MINUIT2 routines provided by the Phython `iminuit` package [52].

First, using the full spectrum obtained with the SRIM energy-loss model, we considered a few variants of the R-matrix model differing by the assumed levels through which the β decay proceeds. They are listed in Table I together with the minimized value of χ^2_L per number of degrees of freedom. We reproduce the observation made in Ref. [9] that while two levels are concerned, the model with two $3/2^+$ states reproduces the measured spectrum significantly better than the model with $3/2^+$ and $1/2^+$ states. Since in the level scheme of ^{11}B (Fig. 1) there are three levels that could be involved in the $\beta\alpha$ process, we tested also three-level scenarios. Adding the third $3/2^+$ level does improve the quality of the fit. However, if we assume the third level to be $1/2^+$, as tentatively assigned to the state at 9820 keV [5], we obtain the best overall description of the data. Thus, for further consideration, we take only the models with two $3/2^+$ levels and two $3/2^+$ plus one $1/2^+$ levels.

TABLE I. Four major R-matrix models fitted to the $\beta\alpha$ spectrum of ^{11}Be. Minimized value of χ^2_L divided by the number of degrees of freedom is shown in the second column.

Model	χ^2_L/ndf
$3/2^+ + 1/2^+$	13.81
$3/2^+ + 3/2^+$	5.03
$3/2^+ + 3/2^+ + 1/2^+$	2.21
$3/2^+ + 3/2^+ + 3/2^+$	3.10

TABLE II. Results of different variants of the two selected R-matrix models fitted to the $\beta\alpha$ spectrum of ^{11}Be. The second column indicates if the full experimental spectrum was taken or the one with removed events having small emission angles, see text for details. Level energies are in keV. Numbers in parentheses denote statistical errors.

Model	Variant	χ^2_L/ndf	E_1	E_2	E_3
$2\times 3/2^+$	full	5.03	9906(1)	11795(100)	-
	removed	3.02	9901(1)	11682(75)	-
$2\times 3/2^+ + 1/2^+$	full	2.21	9923(4)	11817(100)	9813(20)
	removed	1.64	9912(6)	11672(200)	9810(25)

In the next step, we checked how the final results will change if we remove from the SRIM experimental spectrum events having the emission angle in the range $(-20°, -5°)$, which contains a large part of misidentified angles, as shown in Fig. 14b. The results of this exercise are shown in Table II. It can be seen that for both R-matrix models the fit is improved when the events having small negative emission angles are removed, leaving 180 556 events in the spectrum. Again, the best result overall is achieved for the R-matrix model with two $3/2^+$ plus $1/2^+$ levels. The two best fits are shown in Fig. 15.

From the best-fitted parameters, in addition to the level energy, we can deduce the level widths and quantities characterising β decay of ^{11}Be. Instead of reduced width amplitudes $\gamma_{\lambda c}$, we present their ratio to the Wigner limit [53]:

$$\theta^2_{\lambda c} = \frac{\gamma^2_{\lambda c}\,\mu a_c^2}{\hbar^2}, \qquad (5)$$

where μ is the reduced mass of ^{7}Li and α particle and a_c is the channel radius, $a_c = r_0\,(A_1^{1/3} + A_2^{1/3})$. The observed width of

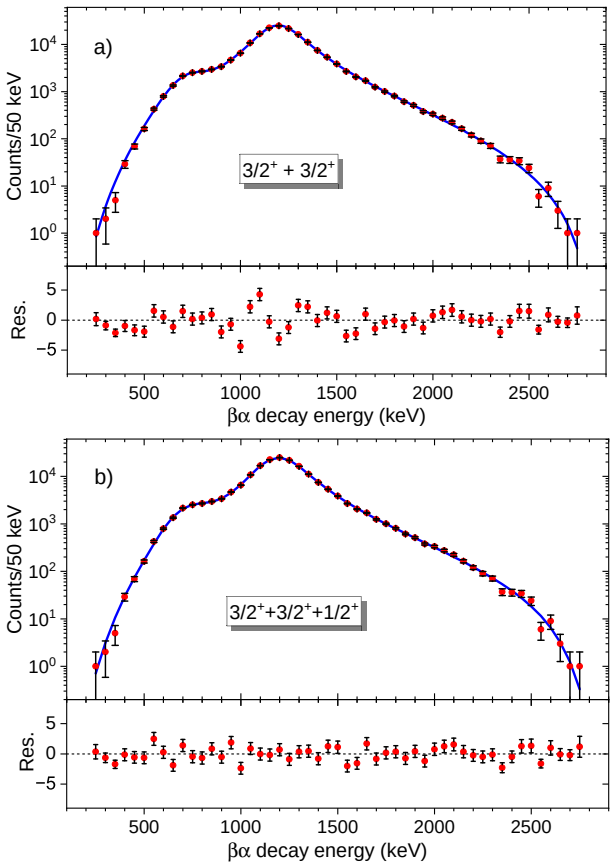

FIG. 15. (Color online) Measured $\beta\alpha$ spectrum of ^{11}Be (red points with error bars) compared to best R-matrix fits (blue line). Data come from the SRIM-model reconstruction with removed events having the emission angle in the range $(-20°, -5°)$. In the bottom parts, the fit residuals, $(n_i - y_i)/\sqrt{y_i}$, are shown. The models assuming two $3/2^+$ (a) and two $3/2^+$ plus one $1/2^+$ (b) levels in ^{11}B are presented.

the level is given by [48]:

$$\Gamma_\lambda = \sum_c \Gamma_{\lambda c},$$
$$\Gamma_{\lambda c} = \frac{2P_c\gamma_{\lambda c}^2}{1+\sum_c \gamma_{\lambda c}^2 \frac{dS_c}{dE}\Big|_{E_\lambda}}, \quad (6)$$

where S_c is the R-matrix shift function [46]. The Gamow-Teller matrix elements can be determined approximately [47] from:

$$M_{GT,\lambda} = \left(\frac{\pi D}{N t_{1/2}}\right)^{\frac{1}{2}} \left(1+\sum_c \gamma_{\lambda c}^2 \frac{dS_c}{dE}\Big|_{E_\lambda}\right)^{-\frac{1}{2}} B_\lambda, \quad (7)$$

where $D = 6147(2)$ s [54], $t_{1/2}$ is the partial half-life for the $\beta\alpha$ decay, and N is the number of counts in the spectrum. More often used quantities B_{GT} and $\log(ft)$ follow:

$$B_{GT,\lambda} = \left(\frac{g_A}{g_V}\right)^{-2} M_{GT,\lambda}^2; \quad \log(ft)_\lambda = \log\left[\frac{D}{M_{GT,\lambda}^2}\right], \quad (8)$$

where $|\frac{g_A}{g_V}| = 1.2723(23)$ [55]. All results for the two best fits are listed in Table III together with values published in Ref. [9] which corresponds to the R-matrix model with two $3/2^+$ levels.

TABLE III. Best fit parameters and derived quantities for two R-matrix models found to best reproduce the $\beta\alpha$ spectrum determined in this work, compared to the results of Ref. [9]. In parentheses, the statistical errors are given, while in square brackets the systematical errors are shown.

	$2\times3/2^+$ Ref. [9]	$2\times3/2^+$	$2\times3/2^+ + 1/2^+$
E_1 (keV)	9 846(1)[10]	9 901(1)[30]	9 912(6)[35]
$B_1/\sqrt{N}$	0.161(2)	0.152(1)[2]	0.140(10)[3]
θ_{11}^2	1.31(2)	1.04(1)[17]	0.92(6)[14]
θ_{12}^2	0.84(2)	0.44(1)[13]	0.42(3)[14]
Γ_{11} (keV)	233(3)[3]	263(2)[4]	251(4)[7]
Γ_{12} (keV)	20.4(3)[3]	18.9(3)[2]	20(1)[1]
M_{GT_1}	0.717(12)[7]	0.760(2)[40]	0.714(20)[25]
B_{GT_1}	0.318(11)[6]	0.357(2)[35]	0.315(15)[20]
$\log(ft)_1$	4.08(3)[2]	4.027(2)[40]	4.08(2)[3]
E_2 (keV)	11 490(80)[50]	11 682(75)[260]	11 672(200)[40]
$B_2/\sqrt{N}$	0.156(26)	0.160(4)[70]	0.09(4)[20]
θ_{21}^2 [a]	-0.21(7)	-0.152(25)[60]	-0.39(13)[30]
θ_{22}^2 [a]	0.029(37)	0.015(16)[25]	-0.01(5)[5]
Γ_{21} (keV)	430(150)[50]	338(64)[120]	854(200)[670]
Γ_{22} (keV)	50(60)[50]	27(28)[30]	18(50)[90]
M_{GT_2}	1.05(17)[5]	1.08(3)[50]	0.63(13)[120]
B_{GT_2}	0.7(2)[1]	0.72(4)[80]	0.25(10)[200]
$\log(ft)_2$	3.8(3)[1]	3.72(2)[30]	4.2(2)[10]
E_3 (keV)			9 810(25)[40]
$B_3/\sqrt{N}$			0.042(22)[15]
θ_{31}^2			0.61(27)[10]
θ_{32}^2			0.33(3)[15]
Γ_{31} (keV)			146(32)[25]
Γ_{32} (keV)			9(3)[6]
M_{GT_3}			0.23(5)[6]
B_{GT_3}			0.032(15)[20]
$\log(ft)_3$			5.1(2)[2]

[a] The sign in these entries indicates the sign on the corresponding reduced width amplitude, $\gamma_{\lambda c}$.

Statistical errors given in Table III were calculated using covariance matrices provided by the fitting package. The main systematic error in our analysis is related to energy determination. It has two sources. One comes directly from the energy-loss models. Some hint of this contribution is given by the difference between the SRIM and the GEANT4 models, which amounts to $\sim$ 15 keV at the decay energy of 1200 keV. The second source is the uncertainty of the OTPC gas density which is affected by changes of the temperature and pressure, and the inaccuracy of the gas-flow rate from which the gas composition is determined. The estimated overall accuracy of the gas density is about 1% and this leads to an energy shift of

30 keV for a $\beta\alpha$ event at 1200 keV. We adopted this value as the measure of systematic error of energy and we assumed that it grows linearly with increasing energy. Then we changed the bin energies correspondingly and refitted the spectra with the R-matrix models. The resulting changes of the fit parameters were used to determine the systematic errors shown in Table III in square brackets.

Our results support one of the main conclusions of Ref. [9], namely that the satisfactory description of the $\beta\alpha$ spectrum from ^{11}Be requires at least two $3/2^+$ states. Moreover, the β-decay strengths, expressed by the B_{GT} or $\log(ft)$ values, coincide within the error bars with the values determined in Ref. [9]. The energy of E_1, the state dominating the $\beta\alpha$ emission, and its width are very close to the values given in [9], although they are a bit larger. Our value for E_1 is consistent with the known $3/2^+$ level in ^{11}B at 9873 keV (see Fig. 1). The width of this state, however, appears almost three times larger than 109(14) keV measured for the 9873 keV state in scattering and reaction experiments [5]. The energy of our second $3/2^+$ level suggests that it could be the known state at 11450 keV tentatively assigned as $3/2^+$. Unfortunately, our value has a large systematical uncertainty resulting from the rather small contribution to the spectrum. The measured width for this state is smaller than the one found in Ref. [9] but it is still more than three times larger than 93(17) keV adopted for the 11450 keV level [5]. Whether the two states we see in the $\beta\alpha$ emission do coincide with the 9873 keV and 11450 keV levels requires further, independent investigations.

The quality of the R-matrix fit improves if we add a $1/2^+$ state. As a result of this step, all parameters of the first state and the energy of the second state do not change significantly. The width of the second state increases a lot and its β feeding decreases, but they are not well determined having large errors. The third state appears with a width of the order of 150 keV and its energy of 9810 keV is close to the known state in ^{11}B at 9820(25) keV which is tentatively assigned as $1/2^+$ (see Fig. 1). Up to now, the only evidence for this state came from quasi-elastic electron scattering on ^{12}C [56]. Independent confirmation of the energy, spin, and width of this state would be helpful. It is important to note that, as can be seen in Fig. 15, the improvement of the R-matrix fit by adding the $1/2^+$ state comes mainly from the energy region 900–1400 keV. The spectrum in this region is not affected by our, somewhat arbitrary, selection of good $\beta\alpha$ events.

Having the best-fitted R-matrix models, we can determine the branching ratio for the two $\beta\alpha$ decay channels by integrating their contributions to the final spectrum over the whole energy range. For the transition to the ^{7}Li ground state and to the excited state at 478 keV, we found the branching ratios to be 93.7(4)% and 6.3(4)%, respectively, in the two $3/2^+$ levels scenario. For the model with the three levels ($3/2^+ + 3/2^+ + 1/2^+$), the corresponding values are 92.9(3)% and 7.1(3)%. These numbers are close to the results of Ref. [9] which are 92.1(3)% and 7.9(3)%, respectively.

C. Search for βp decay channel

Candidates for the β-delayed proton emission were looked for among those events which were better fitted as βp events than $\beta\alpha$ in the reconstruction procedure. More precisely, all events that were discarded from the $\beta\alpha$ spectrum, i.e. those above the red line in Fig. 13, were taken into account. They consist predominantly of events with $\Delta\chi^2 > 0$ but they include also events with $\Delta\chi^2 \lesssim 0$. The latter have to be considered because at low energy the track profiles of the two types of particle decays (^{7}Li+α and ^{10}Be+p) become similar to each other and it is hard to tell them apart. As reported above, all these events were carefully inspected one by one and those which bore clear signs of damage were removed. Among the removed events, the majority represented a track apparently cut, thus indicating a particle hitting the cathode or the GEM section and thus depositing only a part of its energy in the detector. Another numerous category contained events of equal, sharply defined vertical length, thus suggesting a decay between the GEM foils. In addition, we observed some events with other types of distortions, like a double-bump structure, or resulting apparently from a spark in the GEM structure. All removed events looked very different than expected for the β-delayed emission of protons or α particles. We observed also a number of imperfect events, for which it was not obvious whether they should be retained or removed. These events were used to estimate the uncertainty of the selection procedure.

After this selection, about 2200 events remained as candidates for βp events. Nevertheless, they also can represent $\beta\alpha$ events that appear very similar to the βp ones and/or for which the effect of damage was smeared out by the electron diffusion. For illustration, we present two examples from this group. In the first, shown in Fig. 16, the model of the βp emission fits the data clearly better than the $\beta\alpha$ decay scenario. In contrast, the event shown in Fig. 17 is fitted equally well by the two alternative decay modes.

The low-energy part of the energy spectrum of βp candidates, selected as described above, is shown in Fig. 18 with a grey histogram where the uncertainty of the selection procedure is marked with a line pattern. Interestingly, the number of counts in the region around 200 keV is very small. In the work of Ayyad et al. [19] the β-delayed protons emitted from ^{11}Be were reported to be observed in a narrow peak at a decay energy of 196 keV. This peak was interpreted as originating from a narrow resonance in ^{11}B having a width of 12(5) keV. The resulting branching ratio for the βp emission was determined as $(1.3 \pm 0.3) \times 10^{-5}$ [19].

To compare our results with the observation of Ref. [19], we run the GEANT4 simulations in order to see how the reported βp process would show up in our spectrum. A number of βp events were generated with the decay energy having a Gaussian distribution centered at 196 keV with a variance of 12 keV. These events were reconstructed in the same way as the real data were, using the GEANT4 energy-loss model for consistency. The obtained spectrum was then normalized to the number of counts in the full $\beta\alpha$ spectrum (shown in Fig. 14), taking into account the branching ratios of 3.3×10^{-2},

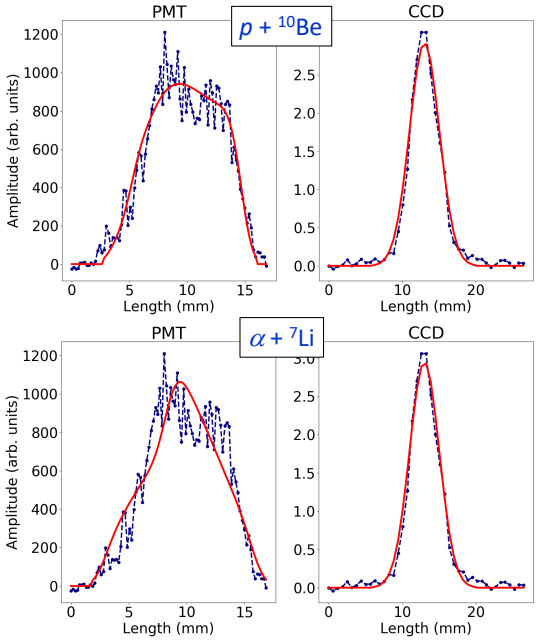

FIG. 16. (Color online) Example event from the group that can contain the βp events. The blue points represent the data, the red lines show the best fit of the model signal. In the top row, the model corresponds to a βp emission with the decay energy of 195 keV and the emission angle of the proton of -83°, while in the bottom row the best-fitted $\beta\alpha$ model is shown with the decay energy of 229 keV and the emission angle of the α particle of 87°.

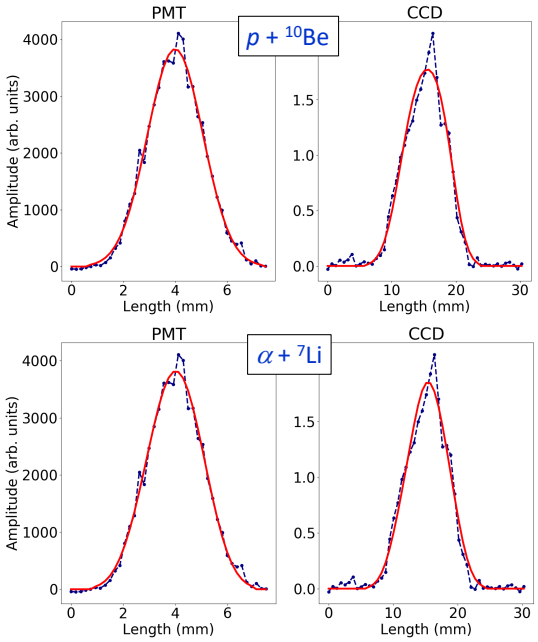

FIG. 17. (Color online) The same as Fig. 16 but for a different event. In the top row, the model corresponds to a βp emission with the decay energy of 176 keV and the emission angle of the proton of 8°, while in the bottom row the best-fitted $\beta\alpha$ model is shown with the decay energy of 190 keV and the emission angle of the α particle of 17°.

and 1.3×10^{-5} for the $\beta\alpha$ and βp emission, respectively. The result is shown in Fig. 18 with the red points while the red band represents the 23% uncertainty of the βp branching ratio determined in Ref. [19]. In total, we should see about (90±20) βp events which is clearly not the case.

For a decay energy below 230 keV, we see in total 15 ± 4 counts. Some of them may belong to the tail of the $\beta\alpha$ background visible in Fig. 18 and there is no unambiguous way to distinguish a good βp event from the distorted $\beta\alpha$ one in this group of events. For example, we see in this group cases that fit well as delayed proton emission, but with the decay energy above 350 keV. Such events cannot represent βp decay for which the maximal energy is 281 keV. Therefore, we can only conclude that for the energy range below 230 keV, the number of βp events in our spectrum is less or equal to $15 \pm 4_{\mathrm{stat}} \pm 4_{\mathrm{sys}}$. This yields an upper limit for the branching ratio of β-delayed proton emission in ^{11}Be of $b_{\beta p} \leq (2.2 \pm 0.6_{\mathrm{stat}} \pm 0.6_{\mathrm{sys}}) \times 10^{-6}$. This value agrees with the limit obtained from the recent indirect measurement of Riisager et al. [27], but is in strong conflict with the result of Ayyad et al. [19]. Since the energy window for the βp emission is opened up to 281 keV, it is possible that a number of βp events are hidden in the $\beta\alpha$ background above 230 keV. We cannot exclude such a possibility, but we note that this would also contradict the observation made in Ref. [19].

Eight events in the energy range 150 – 210 keV may well represent βp decay events. If we tentatively make such an assignment, the branching ratio would be $b_{\beta p} = (1.2 \pm 0.4_{\mathrm{stat}} \pm 0.4_{\mathrm{sys}}) \times 10^{-6}$.

V. SUMMARY AND CONCLUSIONS

We have studied β decay of ^{11}Be with delayed emission of charged particles using the Warsaw TPC detector with optical readout. The β-delayed α emission was investigated in detail. In the experiment carried out at the INFN-LNS the branching ratio for this process was measured by counting incoming ions of ^{11}Be and decay events with emission of particles. From about 2000 decay events recorded, the value of $b_{\beta\alpha} = 3.27(46) \times 10^{-2}$ was determined. This value agrees with the most recent and most accurate value to date, $3.30(10) \times 10^{-2}$ [9], although it has a larger error bar, mainly due to the large uncertainty of the stopping probability of ions in the detector.

In the second experiment, made at the HIE-ISOLDE facility, the energy spectrum of $\beta\alpha$ decay events was measured in the full energy window available for this process. More than

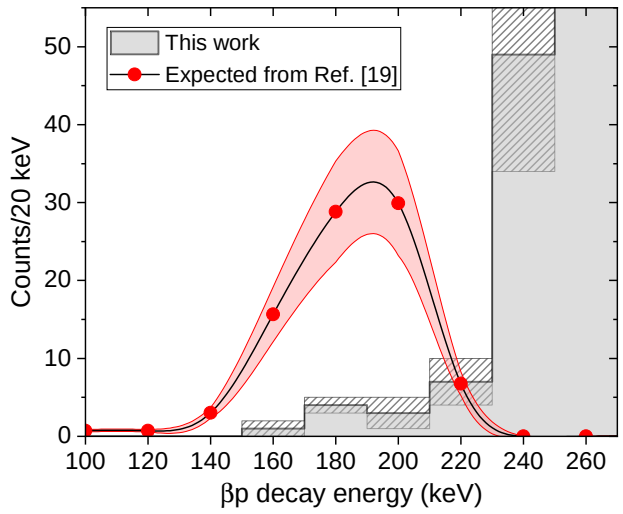

FIG. 18. (Color online) Decay energy spectrum for βp candidate events. The grey histogram shows the data from this work, with the line pattern indicating the uncertainty of the selection procedure. The red points represent the spectrum expected if the β-delayed proton emission in ^{11}Be proceeded as reported in Ref. [19]. The red band illustrates the uncertainty of the claimed βp branching ratio, see text for details.

200 000 counts were recorded and analysed. For the first time the low-energy part of this spectrum, below 500 keV, was obtained. Its detailed shape at lowest energies could have been affected by a background due to distorted signals, most probably because of decays in proximity to the cathode plate or the amplification zone. Nevertheless, the spectrum was found to agree well with the results reported in Ref. [9]. The analysis in the framework of the R-matrix formalism supported the conclusion that at least two $3/2^+$ levels in ^{11}B are needed to satisfactorily reproduce the $\beta\alpha$ spectrum [9]. The energies and log ft values for these states were found consistent with the results of Ref. [9] within the rather substantial systematical errors. One of these states, dominating by far the observed spectrum, at about 9900 keV, probably corresponds to the known $3/2^+$ state at 9873 keV, although the width assigned to it [5] is about 2.5 times narrower than the one observed by us and in Ref. [9]. The energy of the second level, at about 11700 keV was determined with a large systematical error. However, within this uncertainty, it fits to the known state at 11450 keV, tentatively assigned to be a $3/2^+$ [5]. But again, the width deduced by us, as well as in Ref. [9], is more than 3 times larger than the one adopted for the 11450 keV state [5].

We found that a better description of the measured $\beta\alpha$ spectrum in the R-matrix model can be achieved by taking into account a third state of $1/2^+$ nature at about 9800 keV. It appears to be narrower ($\Gamma \approx 150$ keV) than the other two levels. These findings fit to the known state at 9820 keV tentatively assigned as $1/2^+$. Thus, the best description of the measured $\beta\alpha$ spectrum with the R-matrix model is achieved with the pattern of $3/2^+$ and $1/2^+$ states which is very similar to the known level scheme of ^{11}B [5].

The general agreement of our description of the $\beta\alpha$ spectrum from ^{11}Be with the findings of Ref. [9] gives us confidence that our detection technique based on the OTPC detector is well suited for spectroscopic studies of β-delayed charged particle emission even in case of very large number of events. In contrast to experiments using silicon detectors, where the energy is extracted from the signal amplitude only, in our method, each event is reconstructed in detail separately and the energy is determined both from the track length and the energy-deposit distribution along the track. Both approaches have their advantages and both suffer from different systematical errors, thus they should be considered as complementary.

The main goal of this project was to search for the β-delayed proton emission from ^{11}Be. This task was hampered by the presence of a background posed by distorted $\beta\alpha$ events. However, after careful inspection of all events, only 15 of them were found in the energy range where about 90 βp events were expected according to Ref. [19]. From this number, we deduced the upper limit for the βp branching ratio to be $(2.2 \pm 0.6_{\mathrm{stat}} \pm 0.6_{\mathrm{sys}}) \times 10^{-6}$ for the energy below 230 keV. This value is in conflict with the results reported in Ref. [16] and in Ref. [19]. On the other hand, our result agrees with the final limit determined by Riisager et al. [27], though we note that the latter is based on internally conflicting results.

The final answer to the question of whether in the decay of ^{11}Be are protons emitted, and if yes, with which probability, still needs further investigation. A gaseous TPC-like detector seems to be an optimal tool for such studies. For better separation of $\beta\alpha$ events from βp ones, a thinner gas mixture, thus at lower pressure than the one used in the present study would be advantageous, because for longer tracks the differences between the energy-deposition profiles are more pronounced. To minimize the background from distorted $\beta\alpha$ events, bunches of ^{11}Be ions should be implanted in the center of the active volume and the time between consecutive bunches should be large enough for all nuclei to decay in between. These measures would reduce the statistics which could be counterbalanced by using a TPC detector with an electronic readout, where the drift-time waveform is recorded independently for different regions (pads) of the anode. This feature would allow observation of events which are close in time, provided they are sufficiently separated in space.

ACKNOWLEDGEMENTS

We would like to thank the INFN-LNS staff and the ISOLDE Collaboration and technical teams for their support during the experiments and for the excellent quality of the ^{11}Be beam. This work was supported by the Polish Ministry of Science and Higher Education under Contract No. 2021/WK/07, by the National Science Center, Poland, under Contracts No. 2019/33/B/ST2/02908 and No. 2019/35/D/ST2/02081, by the Polish National Agency for Academic Exchange under grant No. PPN/ULM/2019/1/00220 and by the European Union HORIZON2020 research and innovation programme under Grant Agreement No. 654002 - ENSAR2. We acknowledge sup-

port by Spanish MCIN/AEI/ 10.13039/501100011033 under Grants RTI2018-098868-B-I00 and PID2021-126998OB-I00.

* pfutzner@fuw.edu.pl

[1] J. Deutsch, L. Grenacs, J. Lehmann, P. Lipnik, and P. Macq, Physics Letters B **28**, 178 (1968), ISSN 0370-2693, URL https://www.sciencedirect.com/science/article/pii/0370269368900105.

[2] W. Geithner, S. Kappertz, M. Keim, P. Lievens, R. Neugart, L. Vermeeren, S. Wilbert, V. N. Fedoseyev, U. Köster, V. I. Mishin, et al., Phys. Rev. Lett. **83**, 3792 (1999), URL https://link.aps.org/doi/10.1103/PhysRevLett.83.3792.

[3] I. Talmi and I. Unna, Phys. Rev. Lett. **4**, 469 (1960), URL https://link.aps.org/doi/10.1103/PhysRevLett.4.469.

[4] M. Fukuda, T. Ichihara, N. Inabe, T. Kubo, H. Kumagai, T. Nakagawa, Y. Yano, I. Tanihata, M. Adachi, K. Asahi, et al., Physics Letters B **268**, 339 (1991).

[5] J. Kelley, E. Kwan, J. Purcell, C. Sheu, and H. Weller, Nuclear Physics A **880**, 88 (2012), ISSN 0375-9474, URL https://www.sciencedirect.com/science/article/pii/S0375947412000413.

[6] A. Calci, P. Navrátil, R. Roth, J. Dohet-Eraly, S. Quaglioni, and G. Hupin, Phys. Rev. Lett. **117**, 242501 (2016), URL https://link.aps.org/doi/10.1103/PhysRevLett.117.242501.

[7] D. E. Alburger and D. H. Wilkinson, Phys. Rev. C **3**, 1492 (1971), URL https://link.aps.org/doi/10.1103/PhysRevC.3.1492.

[8] D. E. Alburger, D. J. Millener, and D. H. Wilkinson, Phys. Rev. C **23**, 473 (1981), URL https://link.aps.org/doi/10.1103/PhysRevC.23.473.

[9] J. Refsgaard, J. Büscher, A. Arokiaraj, H. O. U. Fynbo, R. Raabe, and K. Riisager, Phys. Rev. C **99**, 044316 (2019), URL https://link.aps.org/doi/10.1103/PhysRevC.99.044316.

[10] M. Wang, W. Huang, F. Kondev, G. Audi, and S. Naimi, Chinese Physics C **45**, 030003 (2021), URL https://dx.doi.org/10.1088/1674-1137/abddaf.

[11] M. Pfützner, M. Karny, L. V. Grigorenko, and K. Riisager, Rev. Mod. Phys. **84**, 567 (2012), URL https://link.aps.org/doi/10.1103/RevModPhys.84.567.

[12] D. Baye and E. Tursunov, Physics Letters B **696**, 464 (2011), ISSN 0370-2693, URL https://www.sciencedirect.com/science/article/pii/S0370269311000281.

[13] B. Jonson and K. Riisager, Nuclear Physics A **693**, 77 (2001), ISSN 0375-9474, radioactive Nuclear Beams, URL https://www.sciencedirect.com/science/article/pii/S0375947400005601.

[14] K. Riisager, Few-Body Systems **58**, 106 (2017), ISSN 1432-5411, URL https://doi.org/10.1007/s00601-017-1270-x.

[15] M. J. G. Borge, L. M. Fraile, H. O. U. Fynbo, B. Jonson, O. S. Kirsebom, T. Nilsson, G. Nyman, G. Possnert, K. Riisager, and O. Tengblad, Journal of Physics G: Nuclear and Particle Physics **40**, 035109 (2013), URL https://dx.doi.org/10.1088/0954-3899/40/3/035109.

[16] K. Riisager, O. Forstner, M. Borge, J. Briz, M. Carmona-Gallardo, L. Fraile, H. Fynbo, T. Giles, A. Gottberg, A. Heinz, et al., Physics Letters B **732**, 305 (2014), ISSN 0370-2693, URL https://www.sciencedirect.com/science/article/pii/S0370269314002299.

[17] B. Fornal and B. Grinstein, Phys. Rev. Lett. **120**, 191801 (2018), URL https://link.aps.org/doi/10.1103/PhysRevLett.120.191801.

[18] M. Pfützner and K. Riisager, Phys. Rev. C **97**, 042501 (2018), URL https://link.aps.org/doi/10.1103/PhysRevC.97.042501.

[19] Y. Ayyad, B. Olaizola, W. Mittig, G. Potel, V. Zelevinsky, M. Horoi, S. Beceiro-Novo, M. Alcorta, C. Andreoiu, T. Ahn, et al., Phys. Rev. Lett. **123**, 082501 (2019), URL https://link.aps.org/doi/10.1103/PhysRevLett.123.082501.

[20] J. Okołowicz, M. Płoszajczak, and W. Nazarewicz, Phys. Rev. Lett. **124**, 042502 (2020), URL https://link.aps.org/doi/10.1103/PhysRevLett.124.042502.

[21] A. Volya, Europhysics Letters **130**, 12001 (2020), URL https://dx.doi.org/10.1209/0295-5075/130/12001.

[22] W. Elkamhawy, Z. Yang, H.-W. Hammer, and L. Platter, Physics Letters B **821**, 136610 (2021), ISSN 0370-2693, URL https://www.sciencedirect.com/science/article/pii/S0370269321005505.

[23] M. C. Atkinson, P. Navrátil, G. Hupin, K. Kravvaris, and S. Quaglioni, Phys. Rev. C **105**, 054316 (2022), URL https://link.aps.org/doi/10.1103/PhysRevC.105.054316.

[24] J. Okołowicz, M. Płoszajczak, and W. Nazarewicz, Journal of Physics G: Nuclear and Particle Physics **49**, 10LT01 (2022), URL https://dx.doi.org/10.1088/1361-6471/ac8948.

[25] N. Le Anh, B. M. Loc, N. Auerbach, and V. Zelevinsky, Phys. Rev. C **106**, L051302 (2022), URL https://link.aps.org/doi/10.1103/PhysRevC.106.L051302.

[26] W. Elkamhawy, H.-W. Hammer, and L. Platter, Phys. Rev. C **108**, 015501 (2023), URL https://link.aps.org/doi/10.1103/PhysRevC.108.015501.

[27] K. Riisager, M. J. G. Borge, J. A. Briz, M. Carmona-Gallardo, O. Forstner, L. M. Fraile, H. O. U. Fynbo, A. G. Camacho, J. G. Johansen, B. Jonson, et al., The European Physical Journal A **56**, 100 (2020), ISSN 1434-601X, URL https://doi.org/10.1140/epja/s10050-020-00110-2.

[28] Y. Ayyad, W. Mittig, T. Tang, B. Olaizola, G. Potel, N. Rijal, N. Watwood, H. Alvarez-Pol, D. Bazin, M. Caamaño, et al., Phys. Rev. Lett. **129**, 012501 (2022), URL https://link.aps.org/doi/10.1103/PhysRevLett.129.012501.

[29] E. Lopez-Saavedra, S. Almaraz-Calderon, B. W. Asher, L. T. Baby, N. Gerken, K. Hanselman, K. W. Kemper, A. N. Kuchera, A. B. Morelock, J. F. Perello, et al., Phys. Rev. Lett. **129**, 012502 (2022), URL https://link.aps.org/doi/10.1103/PhysRevLett.129.012502.

[30] M. Pfützner, W. Dominik, Z. Janas, C. Mazzocchi, M. Pomorski, A. A. Bezbakh, M. J. G. Borge, K. Chrapkiewicz, V. Chudoba, R. Frederickx, et al., Phys. Rev. C **92**, 014316 (2015), URL https://link.aps.org/doi/10.1103/PhysRevC.92.014316.

[31] M. Pomorski, M. Pfützner, W. Dominik, R. Grzywacz, A. Stolz, T. Baumann, J. S. Berryman, H. Czyrkowski, R. Dąbrowski, A. Fijałkowska, et al., Phys. Rev. C **90**, 014311 (2014), URL https://link.aps.org/doi/10.1103/PhysRevC.90.014311.

[32] A. A. Ciemny, C. Mazzocchi, W. Dominik, A. Fijałkowska, J. Hooker, C. Hunt, H. Jayatissa, L. Janiak, G. Kamiński, E. Koshchiy, et al., Phys. Rev. C

106, 014317 (2022), URL https://link.aps.org/doi/10.1103/PhysRevC.106.014317.

[33] F. Sauli, Nuclear Instruments and Methods in Physics Research Section A: Accelerators, Spectrometers, Detectors and Associated Equipment **386**, 531 (1997), ISSN 0168-9002, URL https://www.sciencedirect.com/science/article/pii/S0168900296011722.

[34] P. Russotto, L. Calabretta, G. Cardella, G. Cosentino, E. D. Filippo, B. Gnoffo, M. L. Cognata, N. Martorana, E. Pagano, R. Pizzone, et al., Journal of Physics: Conference Series **1014**, 012016 (2018), URL https://dx.doi.org/10.1088/1742-6596/1014/1/012016.

[35] N. S. Martorana, G. Cardella, C. Guazzoni, E. V. Pagano, A. D. Russo, P. Russotto, L. Acosta, A. Amato, L. Calabretta, A. Caruso, et al., Frontiers in Physics **10** (2022), ISSN 2296-424X, URL https://www.frontiersin.org/articles/10.3389/fphy.2022.1058419.

[36] M. J. G. Borge and B. Jonson, Journal of Physics G: Nuclear and Particle Physics **44**, 044011 (2017), URL https://dx.doi.org/10.1088/1361-6471/aa5f03.

[37] R. Catherall, W. Andreazza, M. Breitenfeldt, A. Dorsival, G. J. Focker, T. P. Gharsa, G. T. J, J.-L. Grenard, F. Locci, P. Martins, et al., Journal of Physics G: Nuclear and Particle Physics **44**, 094002 (2017), URL https://dx.doi.org/10.1088/1361-6471/aa7eba.

[38] Y. Kadi, Y. Blumenfeld, W. V. Delsolaro, M. A. Fraser, M. Huyse, A. P. Koufidou, J. A. Rodriguez, and F. Wenander, Journal of Physics G: Nuclear and Particle Physics **44**, 084003 (2017), URL https://dx.doi.org/10.1088/1361-6471/aa78ca.

[39] V. Fedosseev, K. Chrysalidis, T. Day Goodacre, B. Marsh, S. Rothe, C. Seiffert, and K. Wendt, Journal of Physics G: Nuclear and Particle Physics **44**, 084006 (2017), URL https://dx.doi.org/10.1088/1361-6471/aa78e0.

[40] O. Tarasov and D. Bazin, Nuclear Instruments and Methods in Physics Research Section B: Beam Interactions with Materials and Atoms **376**, 185 (2016), ISSN 0168-583X, proceedings of the XVIIth International Conference on Electromagnetic Isotope Separators and Related Topics (EMIS2015), Grand Rapids, MI, U.S.A., 11-15 May 2015, URL https://www.sciencedirect.com/science/article/pii/S0168583X1600224X.

[41] Y. Prezado, M. Borge, C. Diget, L. Fraile, B. Fulton, H. Fynbo, H. Jeppesen, B. Jonson, M. Meister, T. Nilsson, et al., Physics Letters B **618**, 43 (2005), ISSN 0370-2693, URL https://www.sciencedirect.com/science/article/pii/S0370269305006702.

[42] J. F. Ziegler, M. Ziegler, and J. Biersack, Nuclear Instruments and Methods in Physics Research Section B: Beam Interactions with Materials and Atoms **268**, 1818 (2010), ISSN 0168-583X, http://www.srim.org/, URL https://www.sciencedirect.com/science/article/pii/S0168583X10001862.

[43] S. Agostinelli, J. Allison, K. Amako, J. Apostolakis, H. Araujo, P. Arce, M. Asai, D. Axen, S. Banerjee, G. Barrand, et al., Nuclear Instruments and Methods in Physics Research Section A: Accelerators, Spectrometers, Detectors and Associated Equipment **506**, 250 (2003), ISSN 0168-9002, URL https://www.sciencedirect.com/science/article/pii/S0168900203013688.

[44] A. Allisy, Reports of the International Commission on Radiation Units and Measurements **os-25**, iii (1993), URL https://doi.org/10.1093/jicru_os25.2.iii.

[45] V. Guadilla, N. Sokołowska, and M. Pfützner, Acta Phys. Pol. B Proc. Suppl. **16**, 54 (2023), URL https://www.actaphys.uj.edu.pl/S/16/4-A37.

[46] A. M. Lane and R. G. Thomas, Rev. Mod. Phys. **30**, 257 (1958), URL https://link.aps.org/doi/10.1103/RevModPhys.30.257.

[47] F. Barker and E. Warburton, Nuclear Physics A **487**, 269 (1988), ISSN 0375-9474, URL https://www.sciencedirect.com/science/article/pii/0375947488906136.

[48] C. R. Brune, Phys. Rev. C **66**, 044611 (2002), URL https://link.aps.org/doi/10.1103/PhysRevC.66.044611.

[49] National Nuclear Data Center, LOGFT, https://www.nndc.bnl.gov/logft/, URL https://www.nndc.bnl.gov/logft/.

[50] J. Boersma, Mathematics of Computation **23**, 51 (1969), URL https://doi.org/10.1090/S0025-5718-1969-0237836-7.

[51] S. Baker and R. D. Cousins, Nuclear Instruments and Methods in Physics Research **221**, 437 (1984), ISSN 0167-5087, URL https://www.sciencedirect.com/science/article/pii/0167508784900164.

[52] iminuit documentation, https://iminuit.readthedocs.io/en/stable/.

[53] T. Teichmann and E. P. Wigner, Phys. Rev. **87**, 123 (1952), URL https://link.aps.org/doi/10.1103/PhysRev.87.123.

[54] J. C. Hardy and I. S. Towner, Phys. Rev. C **71**, 055501 (2005), URL https://link.aps.org/doi/10.1103/PhysRevC.71.055501.

[55] M. Tanabashi, K. Hagiwara, K. Hikasa, K. Nakamura, Y. Sumino, F. Takahashi, J. Tanaka, K. Agashe, G. Aielli, C. Amsler, et al. (Particle Data Group), Phys. Rev. D **98**, 030001 (2018), URL https://link.aps.org/doi/10.1103/PhysRevD.98.030001.

[56] G. Van Der Steenhoven, H. Blok, E. Jans, L. Lapikás, E. Quint, and P. De Witt Huberts, Nuclear Physics A **484**, 445 (1988), ISSN 0375-9474, URL https://www.sciencedirect.com/science/article/pii/0375947488903041.